increased cell growth and reduced cell motility (Choi et al., 2013). We previously reported loss of periplakin expression was associated with pathological stage and cancer-specific survival in patients with UCB using immunohistochemical staining (Matsumoto et al., 2014). Periplakin is imperative for maintaining epithelial cell barriers, cellular movement, and attachment in normal physiology (Nagata et al., 2001; Jefferson et al., 2004; Sonnenberg et al., 2007). Normal expression of periplakin would suppress tumor progression; however, when altered, it would allow cancer cells to grow, detach, invade, and gain access to vascular and lymphatic systems.

Overexpression of cyclin A2 has been reported in various malignant tumors, including UCB (Chao et al., 1998; Dobashi et al., 1998; Mrena et al., 2006; Sun et al., 2011). Cyclin A2–induced cisplatin resistance is reflected by the suppression of drug-induced apoptosis. The cyclin A2–mediated reduction in apoptosis was attributable to activation of the phosphatidyl inositol-3-kinase (PI3K)/Akt pathway, which is a major constituent of the mitochondrial anti-apoptotic pathway. The activation of the p-Akt pathway is reportedly one of the mechanisms by which carcinoma cells avoid the effect of chemotherapeutic drugs (Clark et al., 2002; Yang et al., 2006). p-Akt levels were elevated in cisplatin-resistant cells harboring PTEN gene mutation (Gagnon et al., 2004). Because periplakin is known to bind to intermediate filaments and Akt (van den Heuvel et al., 2002), Suzuki et al (Suzuki et al., 2010) showed a direct association of periplakin with Akt. Silencing of periplakin using siRNA significantly reduced basal p-Akt expression, suggesting that the binding of periplakin positively regulated the Akt activity. Interestingly, high expression of p-Akt was associated with high grade and stage of UCB (Sun et al., 2011), and locally advanced or metastatic UCB revealed resistance to cisplatin-based chemotherapy (Ikeda et al., 2011). We found that serum periplakin expression was higher in patients with MIBC than in those with NMIBC, but serum levels in both lesions were significantly decreased compared with that in normal controls. Although previous reports have shown that loss of expression of periplakin associated with pathological stage was seemingly discordant with the present study, both histological and serum expressions of periplakin indicated no or very slight expression in patients with UCB compared with normal controls. Although the precise role of serum periplakin protein in patients with UCB remains unknown, it is possible that biologically aggressive UCB could slightly increase the periplakin protein in serum concordant with the p-Akt pathway, but not to a high level, like that found under normal conditions, and then could progress locally or distantly and survive in anti-cancerous circumstances, for example, floating chemotherapeutic agents in the blood stream.

This study has several limitations. First, the relatively low number of patients did not allow us to show statistical power. Second, this study was performed exclusively in Japan, so more patients of different ethnicities and from countries with different genetic, epigenetic, and environmental risk factors are needed to confirm our results because the proteins of the plakin family are detected as autoantibodies in other lesions (Park et al., 2006; Taille et al., 2011). Third, periplakin is located not only in urothelium but also in other cells. The role of serum periplakin expression needs to be validated in other types of diseases, including cancerous and inflammatory lesions. Finally, the detailed mechanisms and dynamics of periplakin between immunohistochemical staining and serum findings need to be determined.

In conclusion, patients with UCB demonstrated significantly decreased expression of serum periplakin protein compared with normal controls. In addition, we found that serum periplakin expression was higher in patients with MIBC than in those with NMIBC, but serum levels in both lesions were significantly decreased compared with those in normal controls. Further multi-institutional evaluations of serum periplakin in a large patient population are warranted before it can be included in routine clinical use for early detection of UCB. It may be suitable as an adjunct urine cytology and cystoscopy along with a noninvasive diagnostic modality.

Acknowledgements

This study was supported in part by Grant-in-Aid for Scientific Research C (24592408) from The Japan Society for Promotion of Science (to K. Matsumoto). We thank Takuya Ohsawa, MS, for micro-dot blot array support at Kitasato University.

References

Chao Y, Shih YL, Chiu JH, et al (1998). Overexpression of cyclin A but not Skp 2 correlates with the tumor relapse of human hepatocellular carcinoma. *Cancer Res*, **58**, 985-90.

Choi YK, Woo SM, Cho SG, et al (2013). Brain-metastatic triple-negative breast cancer cells regain growth ability by altering gene expression patterns. *Cancer Genomics Proteomics*, **10**, 265-75.

Clark AS, West K, Streicher S, Dennis PA (2002). Constitutive and inducible Akt activity promotes resistance to chemotherapy, trastuzumab, or tamoxifen in breast cancer cells. *Mol Cancer Ther*, **1**, 707-17.

Dobashi Y, Shoji M, Jiang SX, et al (1998). Active cyclin A-CDK2 complex, a possible critical factor for cell proliferation in human primary lung carcinomas. *Am J Pathol*, **153**, 963-72.

Gagnon V, Mathieu I, Sexton E, et al (2004). AKT involvement in cisplatin chemoresistance of human uterine cancer cells. *Gynecol Oncol*, **94**, 785-95.

Ghafouri-Fard S, Nekoohesh L, Motevaseli E (2014). Bladder cancer biomarkers: review and update. *Asian Pac J Cancer Prev*, **15**, 2395-403.

Hatakeyama H, Kondo T, Fujii K, et al (2006). Protein clusters associated with carcinogenesis, histological differentiation and nodal metastasis in esophageal cancer. *Proteomics*, **6**, 6300-16.

Ikeda M, Matsumoto K, Nishi M, et al (2014). Comparison of radical cystectomy and chemoradiotherapy in patients with locally advanced bladder cancer. *Asian Pac J Cancer Prev*, **15**, 6519-24.

Ikeda M, Matsumoto K, Tabata K, et al (2011). Combination of gemcitabine and paclitaxel is a favorable option for patients with advanced or metastatic urothelial carcinoma previously treated with cisplatin-based chemotherapy. *Jpn J Clin Oncol*,

41, 1214-20.
Jefferson JJ, Leung CL, Liem RK (2004). Plakins: goliaths that link cell junctions and the cytoskeleton. *Nat Rev Mol Cell Biol*, **5**, 542-53.
Matsumoto K, Ikeda M, Hirayama T, et al (2014). Clinical value of dividing false positive urine cytology findings into three categories: atypical, indeterminate, and suspicious of malignancy. *Asian Pac J Cancer Prev*, **15**, 2251-5.
Matsumoto K, Ikeda M, Sato Y, et al (2014). Loss of periplakin expression is associated with pathological stage and cancer-specific survival in patients with urothelial carcinoma of the urinary bladder. *Biomed Res*, **35**, 201-6.
Minami S, Nagashio R, Ueda J, et al (2014). Detection of tumor-associated antigens in culture supernatants using autoantibodies in sera from patients with bladder cancer. *Biomed Res*, **35**, 25-35.
Mrena J, Wiksten JP, Kokkola A, et al (2006). Prognostic significance of cyclin A in gastric cancer. *Int J Cancer*, **119**, 1897-901.
Nagata Y, Karashima T, Watt FM, et al (2001). Paraneoplastic pemphigus sera react strongly with multiple epitopes on the various regions of envoplakin and periplakin, except for the c-terminal homologous domain of periplakin. *J Invest Dermatol*, **116**, 556-63.
Nishimori T, Tomonaga T, Matsushita K, et al (2006). Proteomic analysis of primary esophageal squamous cell carcinoma reveals downregulation of a cell adhesion protein, periplakin. *Proteomics*, **6**, 1011-8.
Park GT, Quan G, Lee JB (2006). Sera from patients with toxic epidermal necrolysis contain autoantibodies to periplakin. *Br J Dermatol*, **155**, 337-43.
Shelley MD, Mason MD, Kynaston H (2010). Intravesical therapy for superficial bladder cancer: a systematic review of randomised trials and meta-analyses. *Cancer Treat Rev*, **36**, 195-205.
Sonnenberg A, Liem RK (2007). Plakins in development and disease. *Exp Cell Res*, **313**, 2189-203.
Sun CH, Chang YH, Pan CC (2011). Activation of the PI3K/Akt/mTOR pathway correlates with tumour progression and reduced survival in patients with urothelial carcinoma of the urinary bladder. *Histopathology*, **58**, 1054-63.
Suzuki A, Horiuchi A, Ashida T, et al (2010). Cyclin A2 confers cisplatin resistance to endometrial carcinoma cells via up-regulation of an Akt-binding protein, periplakin. *J Cell Mol Med*, **14**, 2305-17.
Taille C, Grootenboer-Mignot S, Boursier C, et al (2011). Identification of periplakin as a new target for autoreactivity in idiopathic pulmonary fibrosis. *Am J Respir Crit Care Med*, **183**, 759-66.
Toma MI, Friedrich MG, Hautmann SH, et al (2004). Comparison of the ImmunoCyt test and urinary cytology with other urine tests in the detection and surveillance of bladder cancer. *World J Urol*, **22**, 145-9.
Tonoike Y, Matsushita K, Tomonaga T, et al (2011). Adhesion molecule periplakin is involved in cellular movement and attachment in pharyngeal squamous cancer cells. *BMC Cell Biol*, **12**, 41.
Tsumura H, Matsumoto K, Matsumoto T, et al (2014). Increased expression of serum uroplakin III is associated with the detection and pathological features of aggressive bladder cancer. *Eur Urol Suppl*, **13**, 48.
van den Heuvel AP, de Vries-Smits AM, van Weeren PC, et al (2002). Binding of protein kinase B to the plakin family member periplakin. *J Cell Sci*, **115**, 3957-66.
Yang X, Fraser M, Moll UM, et al (2006). Akt-mediated cisplatin resistance in ovarian cancer: modulation of p53 action on caspase-dependent mitochondrial death pathway. *Cancer Res*, **66**, 3126-36.

Biomedical Research (Tokyo) 35 (3) 201-206, 2014

Loss of periplakin expression is associated with pathological stage and cancer-specific survival in patients with urothelial carcinoma of the urinary bladder

Kazumasa MATSUMOTO[1], Masaomi IKEDA[1], Yuichi SATO[2], Hidetoshi KURUMA[3], Yuko KAMATA[3], Takanori NISHIMORI[4], Tsuyoshi TOMONAGA[6], Fumio NOMURA[5], Shin EGAWA[3], and Masatsugu IWAMURA[1]

[1] Department of Urology, School of Medicine and [2] Department of Molecular Diagnostics, School of Allied Health Sciences, Kitasato University, Kitasato 1-15-1, Minami-ku, Sagamihara-shi, Kanagawa 252-0374, Japan; [3] Department of Urology, School of Medicine, Jikei University, Nishi-shinbashi 3-25-8, Minato-ku, Tokyo 105-8461, Japan; Departments of [4] Frontier Surgery and [5] Molecular Diagnosis, Graduate School of Medicine, Chiba University, Inohana 1-8-1, Chuo-ku, Chiba-shi, Chiba 260-8670, Japan; and [6] National Institute of Biomedical Innovation, Laboratory of Proteome Research, Saitoasagi 7-6-8, Ibaraki-shi, Osaka 567-0085, Japan

(Received 31 March 2014; and accepted 11 April 2014)

ABSTRACT

The objective of this study was to determine periplakin expression in normal urothelium and bladder cancer tissues and the relationship to clinicopathological findings. Immunohistochemical staining for periplakin was carried out in 92 archival radical cystectomy specimens, with immunoreactivity being stratified on a 0–6 scale. Immunohistochemical staining for periplakin was shown to be significantly lower in bladder cancer tissues compared to non-cancerous tissues including inflammation, hyperplasia and normal urothelium. Loss of periplakin expression was associated with pathological stage ($P = 0.04$). In multivariate Cox regression analysis, loss of periplakin expression and positive lymph node status were independent prognostic factors for cancer-specific survival ($P = 0.03$ and 0.015; odds ratio = 2.29 and 2.66; 95% confidence interval = 1.085–4.814 and 1.214–5.845, respectively). This new molecular marker may aid in identifying and selecting bladder cancer patients undergoing radical cystectomy who may potentially benefit from neoadjuvant or adjuvant therapy.

Urothelial carcinoma of the urinary bladder (UCB) is one of the common malignant lesions of the genitourinary tract. Muscle invasive UCB is life-threatened lesion and may progress to have distant metastases (8). Pathological findings are the most prevalent prognostic factors, however, biologic aggressiveness has led us to an extensive investigation for more precious and reliable molecular proteins in UCB.

Two-dimensional gel electrophoresis (2-DE) has been performed to identify tumor-associated antigenic proteins which were harvested from surgical tissues. Several novel tumor proteins associated to the presence of malignant lesions were previously found (11). Plakin family is one of the candidates for a tumor marker in patients with UCB (11).

Periplakin is the 195 kDa membrane-associated protein which was initially identified in a pool of soluble cytoplasmic proteins as a precursor of the cornified cell envelope. It is mainly localized in the desmosomes and interdesmosomal plasma membranes of differentiated epidermal keratinocytes (12, 15), where it is believed to play a major role in keratinocyte intercellular adhesion and to be important for maintaining the integrity of skin and other tissues (2, 12). Multiple-tissue RNA analysis has shown that periplakin is highly expressed in cells from a variety of tissues, including those from genitourinary organs (2, 6, 12), and immunofluorescent

Address correspondence to: Kazumasa Matsumoto, M.D., Department of Urology, School of Medicine Kitasato University, 1-15-1 Kitasato, Minami-ku, Sagamihara, Kanagawa 252-0374, Japan
Tel: +81-42-778-9091, Fax: +81-42-778-9374
E-mail: kazumasa@cd5.so-net.ne.jp

staining of periplakin was shown in plasma membrane of bladder urothelium (12). We previously found significantly decreased expression of periplakin based on 2-DE in esophageal squamous cell carcinomas, particularly those in advanced stages (10).

According to previous results (10, 11), we hypothesized that periplakin is biologic marker with prognostic value for UCB patients. Primary objectives of this study were to describe expression pattern of periplakin in UCB and non-cancerous urothelium and to assess the clinicopathological significance of the observed differences in patients with UCB who underwent radical cystectomy.

MATERIALS AND METHODS

Immunohistochemistry and scoring. Immunohistochemistry was performed by immersing formalin-fixed paraffin sections in 0.01 M citrate buffer (pH 6.0), microwaving for 5 min, and cooling to room temperature. Sections were then incubated for 16 h in a humidified chamber at 4°C with a goat anti-human periplakin polyclonal antibody (Santa Cruz Biotech) at a dilution of 1 : 400. The secondary biotinylated horse anti-goat IgG antibody (Vector Laboratories Inc., Burlingame, CA) was used at a dilution of 1 : 200. Normal urothelial cells served as positive controls. Batch negative controls were used by omitting the primary antibodies. All slides were reviewed by a single pathologist (Y.S.) who was blinded to clinical and pathological data.

Each image was scored for immunoreactivity using a 0–3+ semiquantitation system for the intensity of staining and the percentage of positive cells (percentage labeling frequency) (7). The intensity grading scale ranged from no detectable signal [0] to a strong signal seen at low-power magnification [3]. The labeling frequency was scored as 0 (0%), 1 (1–33%), 2 (34–66%), or 3 (67–100%). Protein expression scores were further stratified into strong (scores 4 to 6), slight (scores 1 to 3) and loss (score 0) for presentation purposes, as most UCB specimens were decreased in this antigen.

Patients. We investigated 115 consecutive patients with localized UCB who had undergone radical cystectomy with pelvic and iliac lymphadenectomy between March 1990 and October 2004. In total, 23 patients who had been previously treated with neoadjuvant chemotherapy were excluded. None of the remaining patients were treated preoperatively with either systemic chemotherapy or radiation therapy. The final study group thus comprised 75 males and 17 females, with a median age of 63 years (mean = 62.3 years; range = 40–81 years). Formalin-fixed paraffin-embedded blocks representing the most invasive and representative area of each tumor were collected. The pathological characteristics of the original pathology slides were recorded by a blinded reviewer (Y.S.). The 2002 Tumor–Node–Metastasis (TNM) classification was used for pathological staging, and the World Health Organization classification was used for pathological grading. Lymphovascular invasion (LVI) determined the presence of cancer cells within the endothelial space. Cancer cells that merely invaded a vascular lumen were considered negative.

The median follow-up time was 35.0 months (mean 69.7 months; range 1.1–276.5 months) for those patients who were still alive at the last follow-up session. In total, 17 patients (18.5%) received adjuvant chemotherapy with methotrexate, vinblastine, adriamycin, and cisplatin (MVAC) after surgery for adverse pathological characteristics including regional lymph-node metastases or extra-vesical involvement. A total of 32 patients (34.8%) received MVAC for disease recurrence. The cause of death was determined by a patient's physician, a chart review corroborated by a death certificate, or a death certificate alone. Approval was granted by the ethics committee of Kitasato University School of Medicine and Hospital.

Statistical analyses. For the purposes of our analysis, pathological tumor stage ($\leq$ pT1, pT2, pT3, pT4), grade (grade 1 and 2 versus grade 3), and lymph-node status (N0 versus N1 and N2) were evaluated as dichotomized variables. Chi-square test was utilized to assess the association of pathological stage. The Fisher's exact test was used to evaluate the association between gender, grade, presence of carcinoma *in situ* (CIS), LVI, and lymph-node status. Multivariate survival analyses were performed with the Cox proportional hazards regression model, controlling for periplakin, pathological stage and grade, presence of LVI, and lymph-node metastases. All analyses were performed with StatView (ver. 5.0; SAS Institute, Cary, NC, USA), and $P < 0.05$ was considered to be statistically significant.

RESULTS

Periplakin expression patterns

Immunohistochemical staining of urothelium from non-cancerous bladders and of UCBs is shown in Fig. 1. The non-cancerous bladder epithelium tissues,

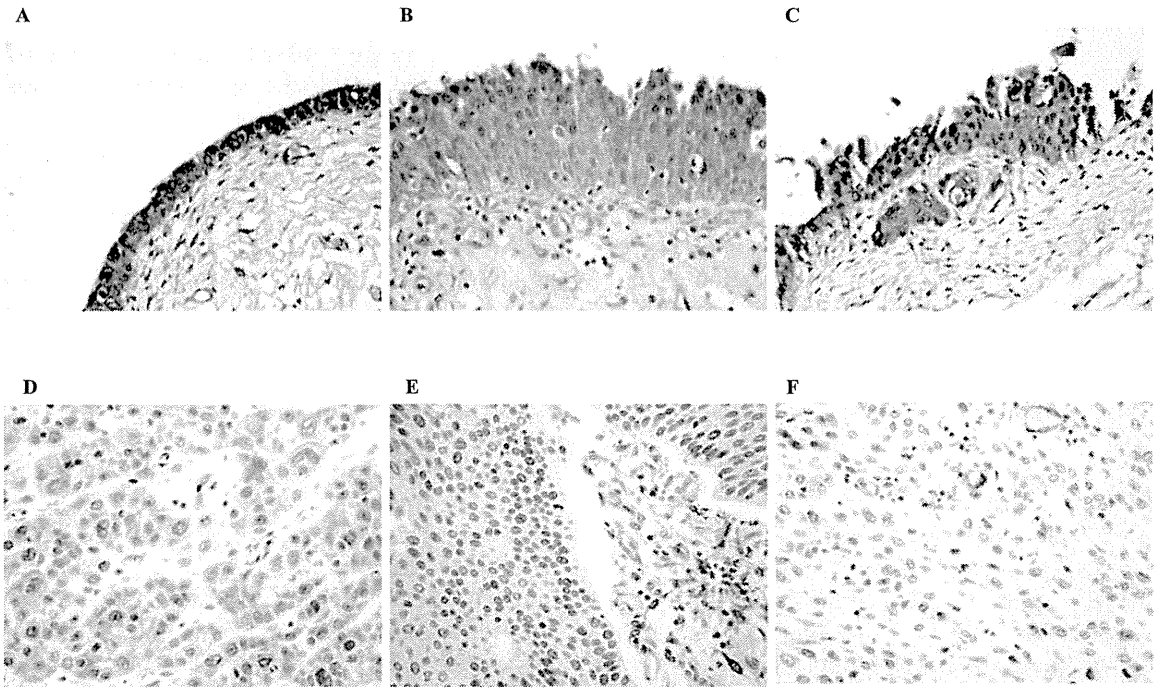

Fig. 1 Immunohistochemical analysis of periplakin expression in non-cancerous tissue and bladder cancer specimens (magnification × 400). Strong periplakin expression was seen in normal urothelium (A), chronic inflammation (B) and urothelial hyperplasia (C). Slight periplakin expression was seen in pT2N0M0 grade 3 cancer tissues (D) and loss of periplakin expression in pT1N0M0 grade 2 (E) and in pT4N0M0 grade 3 cancer tissues (F).

including normal epithelium (Fig. 1A) and specimens exhibiting chronic inflammation (Fig. 1B) and hyperplasia (Fig. 1C), demonstrated strong staining with distinct circumferential and cytoplasmic periplakin immunoreactivity at high intensity. Fibroblasts, smooth muscles, and endothelial cells in blood vessels also showed periplakin immunoreactivity. This periplakin immunoreactivity was significantly reduced in UCBs (Fig. 1D–F).

Association of periplakin expression with clinicopathological findings

Associations between periplakin immunohistochemical expression and clinicopathological findings in the 92 cystectomized patients are shown in Table 1. A complete loss of immunoreactivity was found in 42 (45.7%) of the 92 tumors, and faint expression as "slight" was seen in 50 (54.3%). No strong periplakin immunoreactivity was observed in all cases of UCB. Loss of periplakin expression was associated with advanced stage ($P = 0.04$), but there were no associations between periplakin expression and the other clinicopathological findings ($P > 0.05$).

Association of periplakin expression with prognosis

Disease progression was observed in 44 patients (47.8%), and 50 patients (54.3%) died during the study period. Of these 44 patients died of metastatic UCB (88.0%) and six patients died from intercurrent causes without evidence of disease progression. In a multivariate Cox proportional hazards regression analysis of clinicopathological parameters and periplakin status, loss of periplakin expression and lymph-node metastasis were associated with cancer-specific survival ($P = 0.03$ and 0.015; odds ratio (OR) = 2.29 and 2.66; 95% confidence interval (CI) = 1.085–4.814 and 1.214–5.845, respectively), while only lymph-node involvement was found to be associated with recurrence free survival ($P = 0.002$; OR = 3.39; 95% CI = 1.594–7.219) (Table 2).

DISCUSSION

Several studies have searched for molecular markers that might identify progression from normal urothelium to low-grade or high-grade UCB. Identified candidates have included oncogenes, tumor-suppressor genes, and cell-adhesion molecules, but none have proved satisfactory for UCB markers (4, 7, 14). We found periplakin expression to be significantly lower in cancerous tissues than in non-cancerous tissues. In addition, the extent to which periplakin expres-

Table 1 *Association of periplakin expression with patient clinical and pathological characteristics*

	No. of patients (%)	Periplakin expression		
		Slight	Loss	*P* value*
Gender (%)				
Male	75 (81.5)	42 (56.0)	33 (44.0)	
Female	17 (18.5)	8 (47.1)	9 (52.9)	0.59
Pathological stage (%)				
pTa, pTis, pT1	24 (26.1)	16 (66.7)	8 (33.3)	
pT2	21 (22.8)	9 (42.9)	12 (57.1)	
pT3	32 (34.8)	11 (34.4)	21 (65.6)	
pT4	15 (16.3)	4 (26.7)	11 (73.3)	0.04**
Pathological grade (%)				
Grades 1 and 2	46 (50.0)	25 (54.3)	21 (45.7)	
Grade 3	46 (50.0)	25 (54.3)	21 (45.7)	0.99
Carcinoma *in situ* (%)				
Negative	77 (83.7)	40 (51.9)	37 (48.1)	
Positive	15 (16.3)	10 (66.7)	5 (33.3)	0.39
Lymph node status (%)‡				
N0	66 (71.7)	33 (50.0)	33 (50.0)	
N1, N2	20 (21.7)	12 (60.0)	8 (40.0)	0.25
LVI status (%)§				
Negative	33 (35.9)	19 (57.6)	14 (42.4)	
Positive	45 (48.9)	23 (51.1)	22 (48.9)	0.65

LVI: lymphovascular invasion. * Fisher's exact test (two-sided). ** Chi-square test. ‡ Six patients with unknown pathological status of lymph node. §Fourteen patients had no lymphovascular status.

Table 2 *Multivariate Cox proportional hazards regression analyses for prediction of recurrence and survival of bladder cancer*

	Recurrence free survival		Cancer specific survival	
	OR (95% CI)	*P* value	OR (95% CI)	*P* value
Periplakin expression	1.59 (0.804–3.136)	0.183	2.29 (1.085–4.814)	0.030
Pathological stage	2.22 (0.831–5.944)	0.111	1.87 (0.689–5.072)	0.219
Pathological grade	1.57 (0.732–3.354)	0.248	1.33 (0.598–2.968)	0.483
Lymph node status	3.39 (1.594–7.219)	0.002	2.66 (1.214–5.845)	0.015
LVI status	1.36 (0.617–2.981)	0.448	1.52 (0.694–3.314)	0.297

OR: odds ratio, CI : confidence interval, LVI : lymphovascular invasion.
Multivariate Cox proportional hazards regression analysis was used to estimate OR with the corresponding 95% CI.

sion was lost was associated with pathological stage and cancer-specific survival. On the other hands, we observed no association between the extent of decreased periplakin expression and any clinicopathological finding other than pathological stage. A possible reason is due to the significant reduction in periplakin expression in UCBs. Thus, determination of periplakin expression levels in surgical specimens of UCB could aid in identifying and selecting those UCB patients undergoing radical cystectomy who may potentially benefit from neoadjuvant or adjuvant therapy.

As inactivation of cell-adhesion molecules is thought to be important for cancer progression and metastases (7, 14), decreased periplakin expression could be a key mechanism in the development of bladder cancer. The full-length 6.2 kb cDNA of periplakin gene encodes a polypeptide with characteristic plakin-like domain organization, including a short carboxyterminal tail with a high degree of homology to other members of the plakin family which are also indispensable for the function and maintenance of the normal stratified epithelium (3, 13). The periplakin gene was mapped using a radiation hybrid panel to human chromosome 1p13.3, and the corresponding mouse gene was mapped by interspecific

backcross analysis to a syntenic region of mouse chromosome 16 (2). However, targeted inactivation of the mouse periplakin gene showed that its expression is not crucial for cell envelope formation or epithelial barrier function (1). Elimination of components of periplakin resulted in no discernible phenotype or carcinogenesis (1), suggesting that the association between periplakin and carcinogenesis might be mediated by other oncogenic factors. Although the possible functional consequences of periplakin overexpression have been suggested previously (2, 5), there have so far been no reports on decreased periplakin and its association with carcinoma development. It is possible that periplakin becomes cross-linked to the cell envelope by default as a mechanism for its disposal during urothelial differentiation (1), but the role of endogenous periplakin in urothelial cells remains unknown.

Cystoscopy and urine cytology are effective diagnostic tools for the detection of UCBs. However, although flexible cystoscopy has made examination more acceptable to patients, it remains an invasive procedure. Urine cytology also has limitations, including insufficient sensitivity and difficulty in quantification (9). In the current study, periplakin protein expression was decreased in the majority of UCB tissues and therefore could be utilized in urine cytology as a diagnostic tool, particularly for low-grade and early-stage UCBs. In a preliminary study, shed urothelium in urine sample was demonstrated a variety of periplakin expressions, including strong, slight and loss expression (data not shown). Cytological periplakin immunoreactivity as part of urine cytology potentially aided diagnostic information. Using cytological periplakin immunohistochemistry might thus allow patients to avoid cystoscopy. We speculate that investigation of periplakin expression in urine sediment may serve as a method for detecting UCB.

This study is limited by a relatively small sample size and by being retrospective nature. While a single pathologist assessed the immunohistochemical results in a blinded situation, interobserver variance was not performed. Tumor sampling bias may have affected the result in this study. Since the majority of periplakin expression was decreased in UCB specimens, we believe that these results were representative for the aspects of UCB. However, further prospective study is needed to validate our findings.

In conclusion, UCBs demonstrated decreased expression of periplakin protein compared to non-cancerous tissues, including normal urothelium and specimens exhibiting inflammation or hyperplasia. In addition, loss of periplakin expression was associated with pathological stage and was independent prognostic factor for cancer-specific survival. Determination of periplakin expression in pathological samples of UCB could possibly aid in identifying and selecting UCB patients undergoing radical cystectomy who may potentially benefit from additional perioperative therapies. Further investigations are needed to verify whether periplakin is directly or indirectly involved in UCB invasion and progression.

Acknowledgement

This study was supported in part by a Japan Society for the Promotion of Science Grants-in-Aid for Science Research, and grant 24592408. We thank Erina Satoh, BA, for immunohistochemical staining support at Kitasato University.

REFERENCES

1. Aho S, Li K, Ryoo Y, McGee C, Ishida-Yamamoto A, Uitto J and Klement JF (2004) Periplakin gene targeting reveals a constituent of the cornified cell envelope dispensable for normal mouse development. *Mol Cell Biol* **24**, 6410–6418.
2. Aho S, McLean WH, Li K and Uitto J (1998) cDNA cloning, mRNA expression, and chromosomal mapping of human and mouse periplakin genes. *Genomics* **48**, 242–247.
3. Aho S, Rothenberger K, Tan EM, Ryoo YW, Cho BH, McLean WH and Uitto J (1999) Human periplakin: genomic organization in a clonally unstable region of chromosome 16p with an abundance of repetitive sequence elements. *Genomics* **56**, 160–168.
4. Esrig D, Spruck CH, 3rd, Nichols PW, Chaiwun B, Steven K, Groshen S, Chen SC, Skinner DG, Jones PA and Cote RJ (1993) p53 nuclear protein accumulation correlates with mutations in the p53 gene, tumor grade, and stage in bladder cancer. *Am J Pathol* **143**, 1389–1397.
5. Feng GJ, Kellett E, Scorer CA, Wilde J, White JH and Milligan G (2003) Selective interactions between helix VIII of the human mu-opioid receptors and the C terminus of periplakin disrupt G protein activation. *J Biol Chem* **278**, 33400–33407.
6. Kazerounian S, Uitto J and Aho S (2002) Unique role for the periplakin tail in intermediate filament association: specific binding to keratin 8 and vimentin. *Exp Dermatol* **11**, 428–438.
7. Matsumoto K, Shariat SF, Ayala GE, Rauen KA and Lerner SP (2005) Loss of coxsackie and adenovirus receptor expression is associated with features of aggressive bladder cancer. *Urology* **66**, 441–446.
8. Matsumoto K, Soh S, Satoh T, Iwamura M, Ishikawa Y, Ishii T and Baba S (2008) Distribution of lymphatic vessel network in normal urinary bladder. *Urology* **72**, 706–710.
9. Muus Ubago J, Mehta V, Wojcik EM and Barkan GA (2013) Evaluation of atypical urine cytology progression to malignancy. *Cancer Cytopathol* **121**, 387–391.
10. Nishimori T, Tomonaga T, Matsushita K, Oh-Ishi M, Kodera Y, Maeda T, Nomura F, Matsubara H, Shimada H and Ochiai T (2006) Proteomic analysis of primary esophageal squamous

cell carcinoma reveals downregulation of a cell adhesion protein, periplakin. *Proteomics* **6**, 1011–1018.
11. Okusa H, Kodera Y, Oh-Ishi M, Minamida S, Tsuchida M, Kavoussi PK, Matsumoto K, Satoh T, Iwamura M, Maeda T and Baba S (2008) Searching for new biomarkers of bladder cancer based on proteomics analysis. *J Electrophoresis* **52**, 19–24.
12. Ruhrberg C, Hajibagheri MA, Parry DA and Watt FM (1997) Periplakin, a novel component of cornified envelopes and desmosomes that belongs to the plakin family and forms complexes with envoplakin. *J Cell Biol* **139**, 1835–1849.
13. Ruhrberg C and Watt FM (1997) The plakin family: versatile organizers of cytoskeletal architecture. *Curr Opin Genet Dev* **7**, 392–397.
14. Shariat SF, Pahlavan S, Baseman AG, Brown RM, Green AE, Wheeler TM and Lerner SP (2001) E-cadherin expression predicts clinical outcome in carcinoma in situ of the urinary bladder. *Urology* **57**, 60–65.
15. Simon M and Green H (1984) Participation of membrane-associated proteins in the formation of the cross-linked envelope of the keratinocyte. *Cell* **36**, 827–834.

Haploinsufficiency of the *c-myc* transcriptional repressor *FIR*, as a dominant negative-alternative splicing model, promoted p53-dependent T-cell acute lymphoblastic leukemia progression by activating Notch1

Kazuyuki Matsushita[1,2,*], Kouichi Kitamura[1,2,*], Bahityar Rahmutulla[1], Nobuko Tanaka[1], Takayuki Ishige[1,2], Mamoru Satoh[1], Tyuji Hoshino[3], Satoru Miyagi[4], Takeshi Mori[5], Sakae Itoga[2], Hideaki Shimada[6], Takeshi Tomonaga[7], Minoru Kito[8], Yaeko Nakajima-Takagi[4], Shuji Kubo[9], Chiaki Nakaseko[10], Masahiko Hatano[11], Takashi Miki[12], Masafumi Matsuo[5,13], Masaki Fukuyo[14], Atsushi Kaneda[14], Atsushi Iwama[4] and Fumio Nomura[1,2]

[1] Department of Molecular Diagnosis, Graduate School of Medicine, Chiba University, Chiba City, Inohana, Chiba, Japan

[2] Division of Laboratory Medicine, Chiba University Hospital, Chiba City, Inohana, Chiba, Japan

[3] Department of Physical Chemistry, Graduate School of Pharmaceutical Sciences, Chiba University, Inohana, Chiba, Japan

[4] Department of Cellular and Molecular Medicine, Graduate School of Medicine, Chiba University, Inohana, Chuo-ku, Chiba, Japan

[5] Department of Pediatrics, Graduate School of Medicine, Kobe University, Kusunoki-cho, Kobe, Japan

[6] Department of Surgery, School of Medicine, Toho University, Omori-nishi, Ota-ku, , Tokyo, Japan

[7] Laboratory of Proteome Research, National Institute of Biomedical Innovation, Saito-Asagi, Ibaraki City, Osaka, Japan

[8] Oriental Yeast Co., Ltd. Azusawa, Itabashi-ku, Tokyo, Japan

[9] Department of Genetics, Hyogo College of Medicine, Mukogawa-cho, Nishinomiya, Hyogo Prefecture, Japan

[10] Department of Haematology, Chiba University Hospital, Inohana, Chiba, Japan

[11] Department of Biomedical Science, Graduate School of Medicine, Chiba University, Chiba City, Inohana, Chiba, Japan

[12] Department of Medical Physiology, Graduate School of Medicine, Chiba University, Inohana, Chiba, Japan

[13] Department of Medical Rehabilitation, Faculty of Rehabilitation, Kobegakuin University, Arise, Ikawadani, Nishi, Kobe, Japan

[14] Department of Molecular Oncology, Graduate School of Medicine, Chiba University, Inohana, Chiba, Japan

[*] Equal contribution to this study

Correspondence to: *Kazuyuki Matsushita,* ***email:*** *kmatsu@faculty.chiba-u.jp*

Keywords: FBP interacting repressor (FIR), splicing variant, haplo-insufficiency, leukemia, P53, T-ALL

Received: *November 27, 2014* ***Accepted:*** *December 27, 2014* ***Published:*** *December 31, 2014*

This is an open-access article distributed under the terms of the Creative Commons Attribution License, which permits unrestricted use, distribution, and reproduction in any medium, provided the original author and source are credited.

ABSTRACT

FUSE-binding protein (FBP)-interacting repressor (FIR) is a *c-myc* transcriptional suppressor. A splice variant of FIR that lacks exon 2 in the transcriptional repressor domain (FIRΔexon2) upregulates *c-myc* transcription by inactivating wild-type FIR. The ratio of *FIRΔexon2/FIR* mRNA was increased in human colorectal cancer and hepatocellular carcinoma tissues. Because FIRΔexon2 is considered to be a dominant negative regulator of FIR, FIR heterozygous knockout (*FIR*$^{+/-}$) C57BL6 mice were generated. FIR complete knockout (*FIR*$^{-/-}$) was embryonic lethal before E9.5; therefore, it is essential for embryogenesis. This strongly suggests that insufficiency of FIR is crucial for carcinogenesis. *FIR*$^{+/-}$ mice exhibited prominent *c-myc* mRNA upregulation, particularly in the peripheral blood (PB), without any significant pathogenic phenotype. Furthermore, elevated *FIRΔexon2/FIR* mRNA expression was detected in human leukemia samples and cell lines. Because the single knockout of

***TP53* generates thymic lymphoma, *FIR*$^{+/-}$*TP53*$^{-/-}$ generated T-cell type acute lymphocytic/ lymphoblastic leukemia (T-ALL) with increased organ or bone marrow invasion with poor prognosis. RNA-sequencing analysis of sorted thymic lymphoma cells revealed that the Notch signaling pathway was activated significantly in *FIR*$^{+/-}$*TP53*$^{-/-}$ compared with that in *FIR*$^{+/+}$*TP53*$^{-/-}$ mice. *Notch1* mRNA expression in sorted thymic lymphoma cells was confirmed using qRT-PCR. In addition, flow cytometry revealed that *c-myc* mRNA was negatively correlated with *FIR* but positively correlated with *Notch1* in sorted T-ALL/ thymic lymphoma cells. Moreover, the knockdown of *TP53* or *c-myc* using siRNA decreased Notch1 expression in cancer cells. In addition, an adenovirus vector encoding FIRΔexon2 cDNA increased bleomycin-induced DNA damage. Taken together, these data suggest that the altered expression of *FIRΔexon2* increased Notch1 at least partially by activating c-Myc via a TP53-independent pathway. In conclusion, the alternative splicing of FIR, which generates FIRΔexon2, may contribute to both colorectal carcinogenesis and leukemogenesis.**

INTRODUCTION

DNA damage affects carcinogenesis, transcription, alternative splicing, and cell cycle control; however, the precise mechanism behind these affects remains largely unexplored. FUSE-binding protein (FBP) is a transcription factor that stimulates *c-myc* expression [1-3]. FBP-interacting repressor (FIR) is a *c-myc* transcriptional repressor that functions by suppressing the TFIIH/ P89/XPB helicase (P89) [4-7]; hence, enhanced FIR showed antitumor effect in mouse xenografted model by suppressing *c-myc* [8-10]. Markedly , a splice variant of FIR that lacks exon 2 in the transcriptional repression domain (FIRΔexon2) elevates c-Myc protein expression *in vitro* [11]. FIRΔexon2 mRNA is frequently upregulated in human colorectal cancers [12] as well as hepatocellular carcinoma [13], where it stimulates tumor growth by preventing FIR from suppressing *c-myc* [13].FIRΔexon2 functions as a dominant negative regulator of FIR; therefore it reduces FIR function. Recent studies suggested that DNA damage induces alternative splicing of several genes including *FIR* [14,15]. Specifically, FIR/FIRΔexon2 monitors the DNA damage response by potentially interacting with DNA-PKcs or Ku-86 [14]. Therefore, DNA damage may induce persistent *c-myc* upregulation via FIRΔexon2 in cancer cells, whereas it induces TP53 in normal cells

FIR is a splice variant of PUF60, reported as a splicing factor that lacks the exon 5 consists of 17 amino acids [16]. SAP155, a subunit of the SF3b spliceosome complex, interacts directly with PUF60 *in vitro* [17] and could be co-immunoprecipitated with FIR (or FIRΔexon2)-FLAG beads *in vivo* [18].Furthermore, SAP155 is required for proper FIR pre-mRNA splicing; therefore, SAP155-FIR complex formation inhibits the well-established functions of both SAP155 and FIR, disturbing splicing and the transcriptional suppression of *c-myc* [18,19]. Accordingly, the FIR/FIRΔexon2/SAP155 interaction, which affects *FIR* and *p21Kip1* splicing, links the DNA damage response to *c-myc* regulation [19]. In fact SAP155 mutations, which potentially affect FIR/ FIRΔexon2/SAP155 formation, were reported not only in myeloid lineage tumors but also lymphoid lineage tumors [20-23]. Consequently, an aberrant FIR/FIRΔexon2/ SAP155 interaction is responsible for cancer development and differentiation and is a potent target for cancer screening and treatment [13, 19].

The upregulation of c-Myc and Notch1 with TP53 loss-of-function is critical for T-ALL pathogenesis [24]. This mechanism involves the loss of F-box WD repeat-containing protein 7 (FBW7/FBWX7), which was reported to induce sustained c-Myc and Notch1 expression via a post-transcriptional mechanism, resulting in TP53-deficient T-ALL [25, 26]. FBW7 is required for the polyubiquitination-mediated proteasomal degradation of c-Myc. Accordingly, FBW7 modulates leukemia-initiating cell (LIC) activity by regulating c-Myc stability [25], and thereby plays a role in the pathogenesis [26]. However, the mechanism of c-Myc upregulation in T-ALL in the absence of *TP53*, *FBW7*, or *Notch1* mutations is unclear. In this study, the significance of disturbed *FIR* expression was examined by generating *FIR*$^{+/-}$ mice to assess the dominant negative effect of FIRΔexon2. This study indicated that the alternative splicing of FIR links the DNA damage response to *c-myc* regulation and revealed how the alteration of FIR affects c-Myc, Notch1, or TP53 during the pathogenesis of T-ALL in a *FIR*$^{+/-}$*TP53*$^{-/-}$ mouse model.

RESULTS

FIR$^{-/-}$ mice were embryonic lethal at E9.5 or earlier

The design of the FIR-targeting vector (Figure 1A), as well as the wild-type, targeted, and deleted *FIR* alleles used to prepare the *FIR*$^{+/-}$ mice are shown in Figure S1. The *FIR* homozygous knockout mouse *FIR*$^{-/-}$ was prepared by the cross-fertilization of *FIR*$^{+/-}$ mice (Figure

Table 1: The number of FIR hetero and homo knockout mice during the time of observation.

	$FIR^{+/+}$	$FIR^{+/-}$	$FIR^{-/-}$	supposed $FIR^{-/-}$	
Time at obervation	Wild mice	FIR hetero knockout mice	FIR homo knockout mice	Dead embryo	Total
At birth	12	17	0	0	29
E13.5 to E14.5	9	20	0	6	35
E9.5	5	11	0	6	22
Total	26	48	0	12	86

1B). A total of 86 mice were analyzed after the genetically confirmed mating of $FIR^{+/-}$ mice. $FIR^{+/-}$ and $FIR^{+/+}$ were recovered at close to the expected Mendelian ratio of 48:26 (~2:1; Table 1). There were 12 dead embryos (hypothetically $FIR^{-/-}$): six between E13.5 and E14.5 and six on E9.5 (Table 1). No live $FIR^{-/-}$ mice were observed at birth, E13.5–E14.5, or E9.5 (Figure 1B, Table 1). $FIR^{-/-}$ mice exhibited early developmental defects and die by E4.5 or earlier (Dr. David Levens, NCI, USA). *FIR* total knockout, $FIR^{-/-}$, *mouse* is embryonic lethal before E9.5, suggesting that FIR is essential for embryogenesis. Proteins expressed during embryogenesis disappear during development but are re-expressed in cancers [27, 28], suggesting that FIR is crucial for carcinogenesis as well.

$FIR^{+/-}$ mice exhibited increased *c-myc* mRNA expression but had no significant deleterious phenotype

The relative expression of *c-myc* (Figure 1C) and *FIR* (Figure 1D) mRNA in the lungs, intestines, heart, kidney, liver, and peripheral blood (PB) of $FIR^{+/-}$ mouse was approximately half of that detected in wild-type mice. However, $FIR^{+/-}$ mouse had no apparent pathogenic phenotype. Recently, five individuals were reported with *de novo* interstitial 8q24.3 deletions ranging from 65 kb to 1 Mb on the chromosome that includes FIR (PUF60). These deletions had a clinical phenotype that was associated with multiple systemic phenotypes but no hematological malignancy or lymphoma [29, 30]. This suggests that the haploinsufficiency of *PUF60* (*FIR*) with *c-myc* mRNA elevation alone is not sufficient to drive the pathogenesis of T-ALL.

FIR is alternatively spliced in human leukemia

To explore how *c-myc* is activated in T-ALL/lymphoma, the alternative splicing of FIR, the ratio of FIR/FIRΔexon2, and *c-myc* mRNA expression were examined in human leukemia samples (Figure 1E, Table S1). qRT-PCR for the cDNA of full-length FIR variants was performed in bone marrow or peripheral blood samples using primers to amplify the amino terminal region. At least four variants (FIR, PUF60, FIRΔexon2, and PUF60Δexon2) were expected from the alternative use of the two potential exons [12]. The ratio of *FIR*/*FIRΔexon2* mRNA (Figure 1F) was significantly higher in leukemia cells compared with that in non-leukemia or control samples from adults (Figures 1G) and children (data not shown). This suggests that the alternative splicing of *FIR* and the ratio of *FIR*/*FIRΔexon2* may contribute to *c-myc* upregulation in T-ALL. Notably, c-Myc upregulation alone by FIR haploinsufficiency did not generate leukemia. Thus, *FIR* splicing variants rather than *FIR* haploinsufficiency significantly contributes toward promoting the progression of T-ALL/lymphoma via a c-Myc-independent pathway.

$FIR^{+/-}TP53^{-/-}$ promotes the bone marrow invasion of T-cell malignant lymphoma

Because the $FIR^{+/-}$ mice suggested significant *c-myc* upregulation in the PB without a significant pathogenic phenotype, we generated $FIR^{+/-}TP53^{+/-}$ double compound heterozygous knockout mice and cross-fertilized or mated female $TP53^{+/-}$ with male $FIR^{+/-}TP53^{+/-}$ mice because of the low fertility of $FIR^{+/-}TP53^{+/-}$ mice (Figure 2A). The genotypes of the $FIR^{+/-}TP53^{-/-}$ and $FIR^{+/+}TP53^{-/-}$ mice were confirmed by PCR analysis of genomic DNA (Figure 2B). $FIR^{+/-}TP53^{-/-}$ and $FIR^{+/+}TP53^{-/-}$ mice were sacrificed when a loss of 10%–15% bodyweight during growth or a systemic disorder such as dyspnea with a loss of movement was observed. A demonstrative macroscopic view of the organs of $FIR^{+/-}TP53^{-/-}$, $FIR^{+/+}TP53^{-/-}$, and wild-type mice are shown in Figure 2C. Atypical cells in $FIR^{+/-}TP53^{-/-}$ mice that were observed in the PB, bone marrow (BM), liver, spleen, and thymus are shown in Figures 3A and B. Next, flow cytometry analysis of the PB, spleen, thymus, and BM of thymic lymphoma of $FIR^{+/+}TP53^{-/-}$ mice was performed (Figure 3C). These analyses revealed that both $FIR^{+/+}TP53^{-/-}$ *and* $FIR^{+/-}TP53^{-/-}$ mice exhibited T-ALL/T-cell-type thymic lymphoma. Therefore, the single knockout of $TP53^{-/-}$ was sufficient to cause T-ALL/T-cell-type thymic lymphoma. Flow cytometry also revealed that the size of the thymic lymphoma cells was apparently

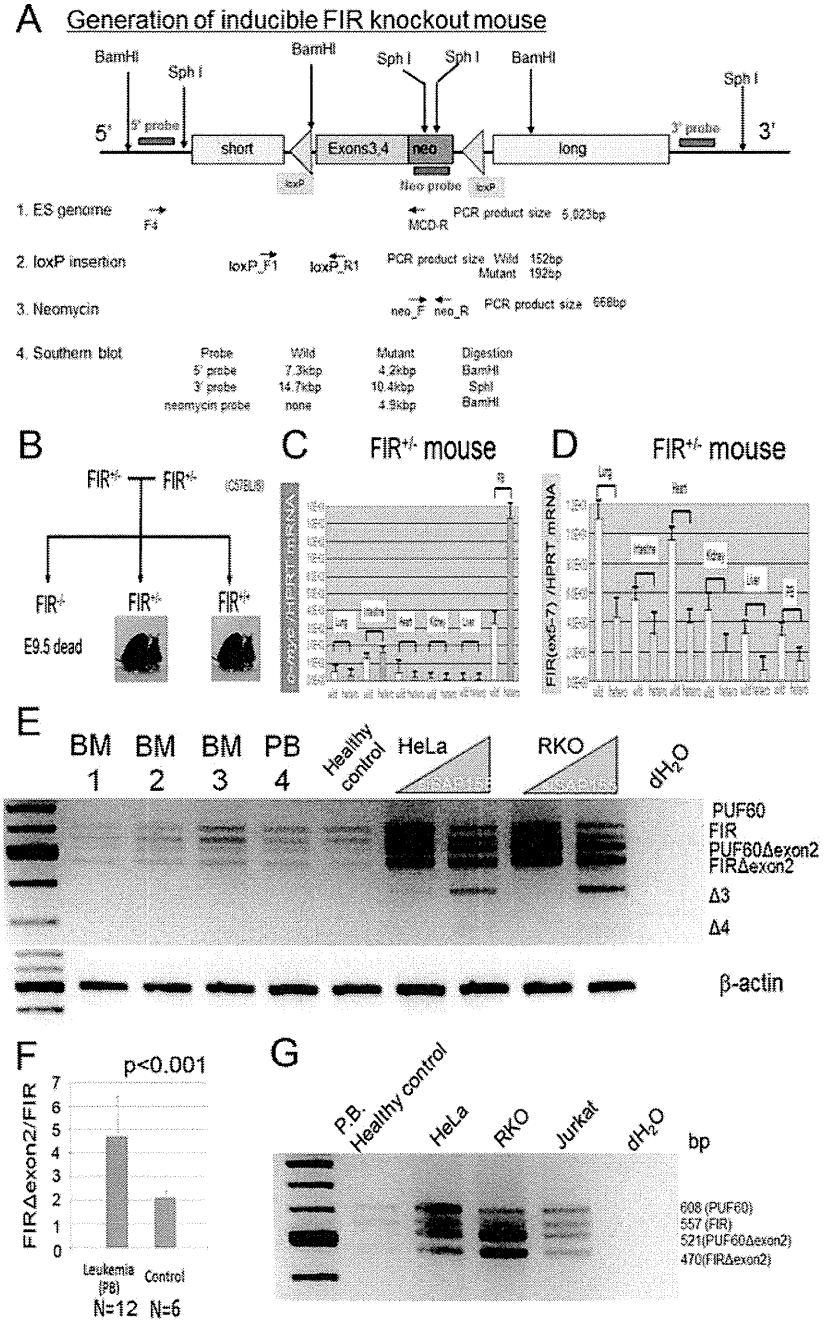

Figure 1: c-Myc mRNA was activated in the peripheral blood cells of inducible FIR heterozygous knockout mouse and FIR/IRΔexon2 mRNA expression in human clinical leukemia/malignant lymphoma samples.(A) Genetic construction for inducible *FIR*$^{+/-}$ mouse. Primers locations for detecting ES genome, LoxP insertion, neomycin cassette and probes for Southern blot analysis were indicated. Expected DNA sizes for Southern blot analysis are also shown. (B) Family tree to obtain FIR homo knockout mouse *FIR*$^{-/-}$, by cross-fertilization between FIR hetero knockout mouse: *FIR*$^{+/-}$. *FIR*$^{-/-}$ mouse was revealed to be embryonic lethal at least before E9.5 by cross-fertilized between FIR hetero knockout mouse. The relative expression of *c-myc* and FIR mRNAs from lung, intestinal mucosae, heart muscle, kidneys, livers and peripheral blood (PB) were examined. (C) *c-myc* mRNA of PB of FIR hetero knockout mice was three-times higher than those of wild mouse. (D) FIR mRNA expression level of FIR hetero knockout mice was exactly half of those of wild mouse. (E) qRT-PCR of PUF60, FIR PUF60Δexon2, FIRΔexon2 mRNA were indicated by RT-PCR. Samples: leukemia cells from peripheral blood (PB) and bone marrow (BM) of adult patients (listed in table 2). (F) The ratio of FIR/FIRΔexon2 mRNA level of leukemia cells was significantly higher than those of non-leukemia or control samples (Student's t-test). (G) mRNA extracted from HeLa (human cervical squamous carcinoma cells), RKO (human colon adenocarcinoma cells), and Jurkat (human immortalized T lymphocyte) cells was examined for their FIR splicing variants expression.

larger in $FIR^{+/-}TP53^{-/-}$ mice compared with that in control mice (Figure 3D, gated area).

Haploinsufficiency of *FIR* developed rapid T-ALL progression with bone marrow invasion

The weight of the thymus was significantly heavier in $FIR^{+/-}TP53^{-/-}$ *and* $FIR^{+/+}TP53^{-/-}$ mice compared with that in wild-type or $FIR^{+/-}TP53^{+/+}$ mice. In addition, the weight of the spleen was significantly heavier in $FIR^{+/+}TP53^{-/-}$ mice than that in wild-type or $FIR^{+/-}TP53^{+/+}$ mice. The WBC count was increased significantly in $FIR^{+/-}TP53^{-/-}$ *and* $FIR^{+/+}TP53^{-/-}$ mice compared with that in wild-type. Conversely, the RBC count was significantly lower in $FIR^{+/+}TP53^{-/-}$ compared with that in wild-type mice. The platelet count was also significantly lower in $FIR^{+/-}TP53^{-/-}$ *and* $FIR^{+/+}TP53^{-/-}$ mice compared with that in wild-type or $FIR^{+/-}TP53^{+/+}$ mice (Figures 4A, B).

$FIR^{+/-}TP53^{-/-}$ mice with T-ALL/lymphoma exhibited a significantly lower bodyweight than did $FIR^{+/+}$ (Figure 4C). One-hundred percent of wild-type and $FIR^{+/-}TP53^{-/-}$ mice survived during the study period, and the overall survival rate (Kaplan–Meier) of $FIR^{+/+}TP53^{-/-}$ mice was better than that of $FIR^{+/-}TP53^{-/-}$ (Figure 4D). There were no significant differences in the nose-to-anus length and bodyweight of $FIR^{+/-}$ compared with that of wild-type mice ($FIR^{+/+}$) (Figure S2). These results suggest that *FIR* haploinsufficiency promoted the progression of T-ALL/lymphoma, reduced bodyweight, and was associated with a poorer prognosis. The incidence of T-ALL with > 10% bone marrow infiltration of blast cells was higher in $FIR^{+/-}TP53^{-/-}$ mice (5 of 23; 21.7%, including three live mice before analysis) compared with that in $FIR^{+/+}TP53^{-/-}$ (1 of 19; 5.3%, including two live mice before analysis) (Figures 4E, F). These results demonstrated that high levels of c-Myc promoted an increased occurrence of T-ALL and bone marrow infiltration in *this mouse model.*

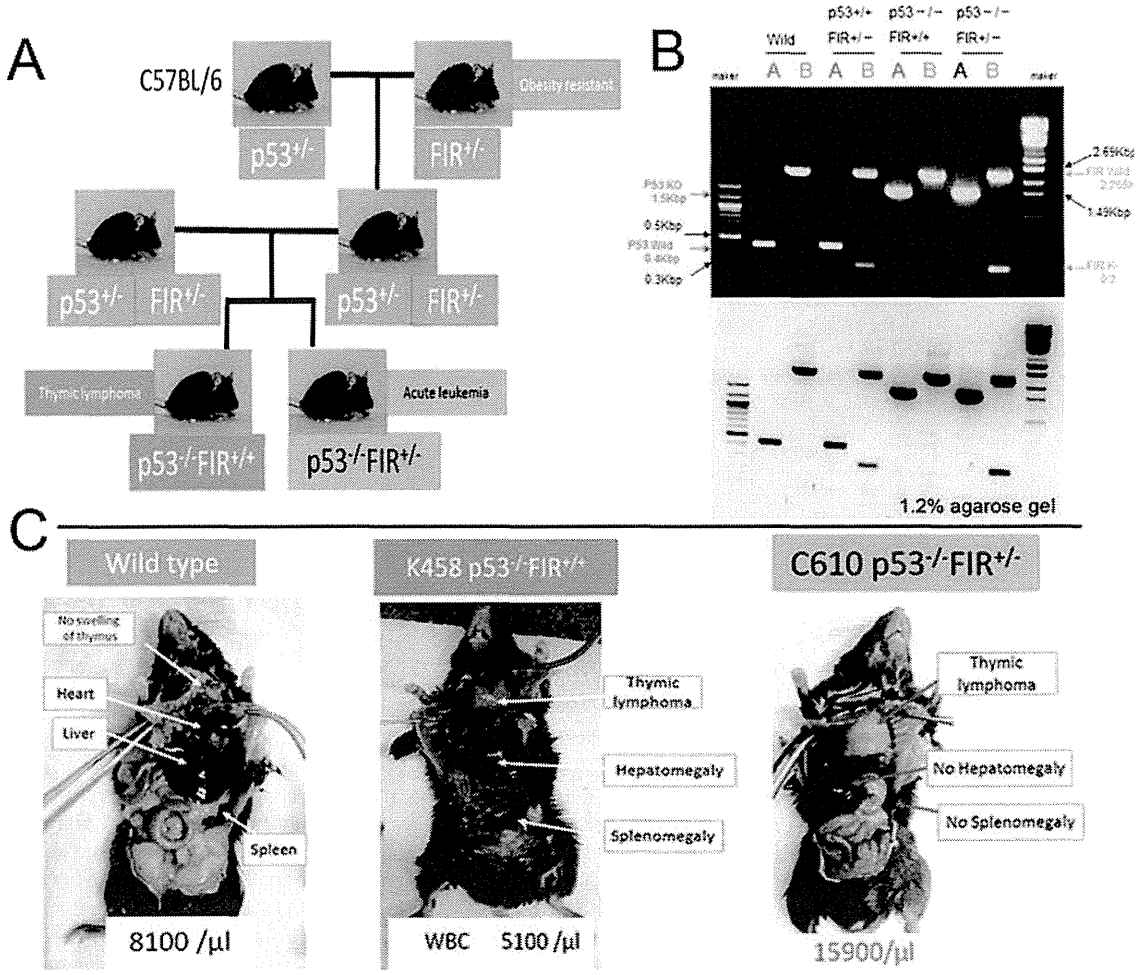

Figure 2: Preparation of $FIR^{+/-}P53^{-/-}$ and $FIR^{+/+}P53^{-/-}$ mouse. (A) $FIR^{+/-}$ and $P53^{-/-}$ were obtained by cross-fertilization between $FIR^{+/-}P53^{-/-}$ and $FIR^{+/+}P53^{-/-}$ mice. $FIR^{+/-}P53^{+/-}$ double compound hetero knockout mouse was prepared and mated each other, or female $P53^{+/-}$ was mated with male $FIR^{+/-}P53^{+/-}$ mouse to obtain $FIR^{+/-}P53^{-/-}$ because $FIR^{+/-}P53^{+/-}$ showed low fertility. (B) Genotyping of $FIR^{+/+}P53^{-/-}$, $FIR^{+/-}P53^{+/+}$ and $FIR^{+/-}P53^{-/-}$ and wild mice were confirmed by PCR. (C) Thymic lymphoma was observed in $FIR^{+/+}p53^{-/-}$ mice.

Of the *FIR*$^{+/-}$*TP53*$^{-/-}$ mice (N = 20), 10 had T-ALL (50.0%), *15* had thymic lymphoma (75%), and five experienced bone marrow invasion (25.0%). In contrast, of the *17* *FIR*$^{+/+}$*P53*$^{-/-}$ mice, seven had T-ALL (41.2%), 10 had thymic lymphoma (58.8%), and one exhibited bone marrow invasion (5.9%) (Figure 4F).

Comparison of RNA-sequencing analysis of sorted thymic lymphoma cells from *FIR*$^{+/-}$*TP53*$^{-/-}$ or *FIR*$^{+/+}$*TP53*$^{-/-}$ mice

RNA-sequencing was used to compare the gene expression profiles of sorted thymic lymphoma cells from FIR$^{+/-}$*TP53*$^{-/-}$ and *FIR*$^{+/+}$*TP53*$^{-/-}$ mice. The top 100 activated genes were analyzed (Figure S3A), and data revealed that the Notch signaling pathway was activated more in CD4^{+}CD8^{+} thymic lymphoma cells from *FIR*$^{+/-}$*TP53*$^{-/-}$ mice compared with those from *FIR*$^{+/+}$*TP53*$^{-/-}$ mice (Table S3A–C). RNA-sequencing analysis of sorted *CD4*$^{+}$*CD8*$^{+}$ thymic lymphoma cells revealed that the Notch signaling (Figure 5) and tight junction pathways (Figure S4A) were activated more significantly in *FIR*$^{+/-}$*TP53*$^{-/-}$ (H635) than *FIR*$^{+/+}$*TP53*$^{-/-}$ (N166) mice. In contrast, analysis of *CD4*$^{low+}$*CD8*$^{+}$ thymic lymphoma cells demonstrated that the focal adhesion pathway (Figure S4B) was activated more significantly in *FIR*$^{+/-}$*TP53*$^{-/-}$ (A605) than in *FIR*$^{+/+}$*TP53*$^{-/-}$ (D619) mice. The upregulation of *c-myc* and *notch1* mRNA was confirmed by qRT-PCR (Table S4, Figure S3C–E). *Notch1* mRNA was more activated in both CD4^{+}CD8^{+} and *CD4*$^{low+}$*CD8*$^{+}$ thymic lymphoma cells from *FIR*$^{+/-}$*TP53*$^{-/-}$ *mice* compared with those from *FIR*$^{+/+}$*TP53*$^{-/-}$ *mice* (Figure S3C, D). In contrast, *c-myc* mRNA was activated in whole peripheral blood cells in two *FIR*$^{+/-}$*TP53*$^{+/+}$ mice examined in this study (Figure S3E).

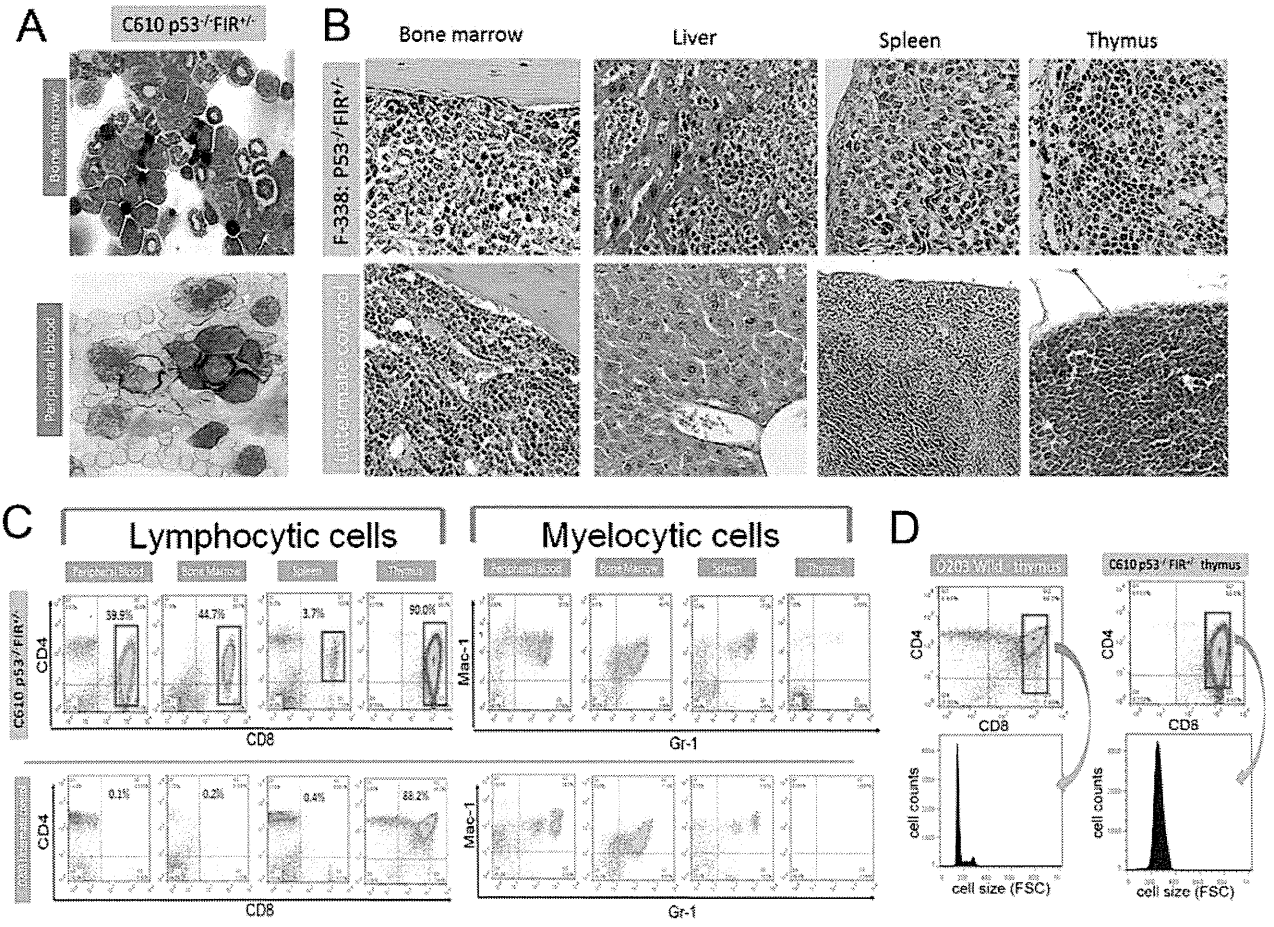

Figure 3: Histologic features and flow cytometry analysis of *FIR*$^{+/-}$*P53*$^{-/-}$. (A) Atypical cells were indicated by Giemsa stain in bone marrow and peripheral blood of *FIR*$^{+/-}$*P53*$^{-/-}$ mouse (C610). (B) Histologic features of bone marrow, liver, spleen and thymus in *FIR*$^{+/-}$*P53*$^{-/-}$ (F338) and wild mouse *by* Hematoxylin-Eosin *stain*. (C) Flow cytometry analysis of lymphocytic cells with CD4 and CD8 as indicated markers. Mac1 and Gr1 were used for myelocytic markers. Flow cytometry analysis revealed that lymphocytic atypical cells (left) were CD4^{low+}CD8^{+} phenotype (gated area) but no significant findings in myeloid cells (right) in *FIR*$^{+/-}$*P53*$^{-/-}$ mouse (C610), and diagnosed as T-cell type acute lymphocytic/lymphoblastic leukemia (T-ALL)/lymphoma. (D) Cell size of gated area was measured by flow cytometry analysis (FSC: Forward Scatter).

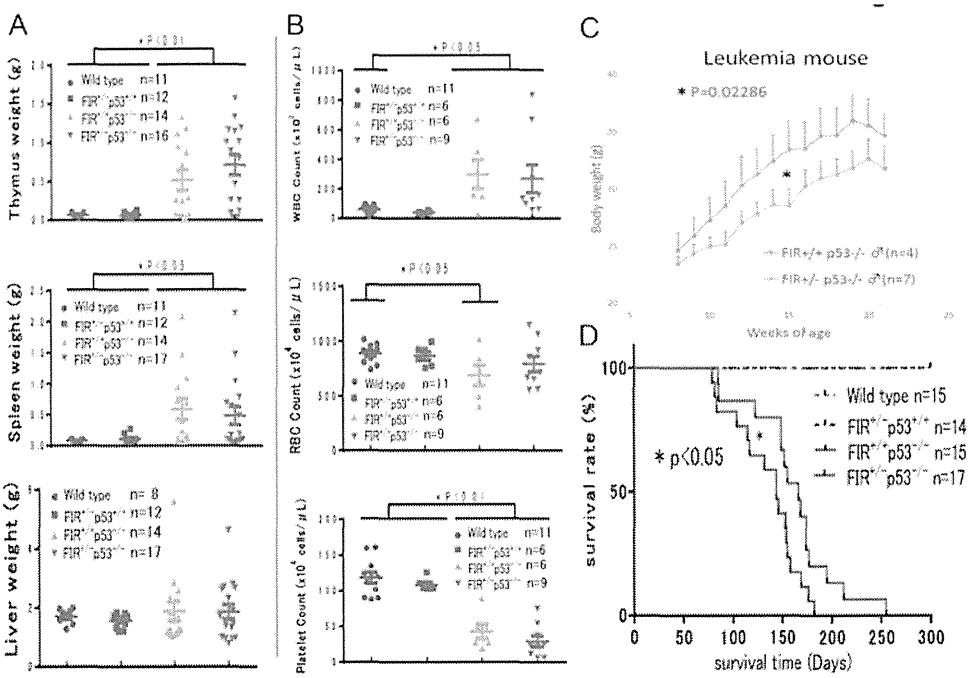

E FIR+/-p53-/- mouse N=23

No.	1	2	3	4	5	6	7	8	9	10	11	12	13	14	15	16	17	18	19	20	Total (%)
Mouse No.	A403	C610	H635	F435	F338	A605	F337	G442	E429	K153	I449	E24	L77	F433	K461	I451	A1	A4	G438	C412	
Leukemia																					50.0
Thymic lymphoma																					75.0
Bone marrow invasion																					25.0
Others																					30.0

Bone marrow invasion>10%, 5/23=21.7%

F FIR+/+p53-/- mouse N=19

No.	1	2	3	4	5	6	7	8	9	10	11	12	13	14	15	16	17	Total (%)
Mouse No.	I450	D619	O490	C10	C16	N166	E428	K132	K464	K458	L75	C122	N485	A2	M52	E335	O324	
Leukemia																		41.2
Thymic lymphoma																		58.8
Bone marrow invasion																		5.9
Others																		47.1

Bone marrow invasion>10%, 1/19=5.3%

Figure 4: Summary of organs' weight and blood tests, body weight and overall survival of curves of *FIR$^{-/-}$P53$^{+/+}$*, *FIR$^{+/-}$P53$^{+/+}$*, *FIR$^{+/+}$P53$^{-/-}$*, and *FIR$^{+/-}$P53$^{-/-}$* mice. (A) The weight of thymus of *FIR$^{+/-}$P53$^{-/-}$ and FIR$^{+/+}$P53$^{-/-}$* was significantly heavier than that of wild or *FIR$^{+/-}$P53$^{+/+}$* mouse (P<0.05). The weight of spleen of *FIR$^{+/+}$P53$^{-/-}$* were significantly heavier than that of wild or *FIR$^{+/-}$P53$^{+/+}$* mouse (P<0.05). The weight of liver of wild mouse, *FIR$^{+/-}$P53$^{+/+}$*, *FIR$^{+/+}$P53$^{-/-}$*, and *FIR$^{+/-}$P53$^{-/-}$* was no significant difference. (B) WBC count of *FIR$^{+/-}$P53$^{-/-}$ and FIR$^{+/-}$P53$^{-/-}$* was significantly increased than that of wild mouse. RBC count of *FIR$^{+/+}$P53$^{-/-}$* was significantly less than that of wild mouse (P<0.05). Platelet count of *FIR$^{+/-}$P53$^{-/-}$ and FIR$^{+/+}$P53$^{-/-}$* was significantly less than that of wild or *FIR$^{+/-}$P53$^{+/+}$* mouse (P<0.05). (C) Body weight of *FIR$^{+/-}$*P53$^{-/-}$ mice was significantly lighter than that of *FIR$^{+/+}$P53$^{-/-}$*. Statistical signifincace was calculated by Student's t-test. (D) The overall survival curves of four genetically different group: wild, *FIR$^{+/-}$p53$^{+/+}$*, *FIR$^{+/-}$p53$^{-/-}$*, and *FIR$^{+/+}$p53$^{-/-}$* mice. *FIR$^{+/-}$p53$^{+/+}$* and *FIR$^{+/+}$p53$^{+/+}$* were survived 100% up to 25 weeks after birth without obvious tumor formation, body weight loss or other physical disabilities. On the contrary, the overall survival curves (Kaplan-Meier method) of *FIR$^{+/-}$p53$^{-/-}$* and *FIR$^{+/+}$p53$^{-/-}$* mice were declined around 70 days after birth. Overall survival curves of four genetically different group: wild, *FIR$^{+/-}$p53$^{+/+}$*, *FIR$^{+/-}$p53$^{-/-}$*, and *FIR$^{+/+}$p53$^{-/-}$* mice were compared by log-rank test. (E) T-ALL with more than 10 % bone marrow infiltration of blast cells in *FIR$^{+/-}$P53$^{-/-}$* mice was 5 out of 23 (21.7%) including three pre-analytical alive mouse *in FIR$^{+/-}$P53$^{-/-}$ (*1 out of 19=5.3%) including two pre-analytical alive mouse. (F) In *FIR$^{+/-}$P53$^{-/-}$* mice *(N=23),* T-ALL: *10 (50.0%),* thymic lymphoma: *15 (75%),* bone marrow invasion: *5 (25.0%).* Whereas in *FIR$^{+/+}$P53$^{-/-}$* mice (N=17) T-ALL: 7 (41.2%), thymic lymphoma: 10 (58.8%), bone marrow invasion: 1 (5.9%). Blank in colored column indicated undetermined or not tested for cell surface marker.

c-Myc and FIR proteins were negatively correlated and *c-myc* and *notch1* mRNAs were positively correlated in sorted thymic lymphoma/ T-ALL cells

Because FIR is believed to be a *c-myc* transcriptional repressor, c-Myc expression was examined in atypical or lymphoma cells from $FIR^{+/-}P53^{-/-}$ mice. As expected, c-Myc expression was higher in atypical/lymphoma cells compared with that in non-atypical cells or normal lymphocytes (Figure 6A). Furthermore, there was a significant negative correlation between *c-myc* and *FIR* mRNA expression in $CD4^+CD8^+$ and $CD4^{low+}CD8^+$ thymic lymphoma cells (Figure 6B). These results strongly suggest that FIR suppresses *c-myc* expression both *in vitro* and *in vivo*. Notably, atypical/lymphoma cells from $FIR^{+/+}TP53^{-/-}$ mice also expressed high levels of c-Myc. These results also suggest that activated *c-myc* mRNA, which does not directly reflect an increase in c-Myc protein, is inadequate for the pathogenesis of T-ALL. Therefore, the pathogenesis of T-ALL/lymphoma observed in $FIR^{+/+}P53^{-/-}$ mice was at least partly *Notch1* upregulation because *c-myc* and *Notch1* mRNAs were positively correlated (Figures 6C, D). Together, the current FIR haploinsufficiency mouse model revealed that T-ALL/ lymphoma was generated via a p53-dependent pathway, but that its progression was potentially due to a c-Myc-independent mechanism because the *TP53* single knockout alone exhibited sustained c-Myc expression.

Knocking down *TP53* and *c-myc* using siRNA suppressed Notch1 expression

Bleomycin (BLM)-induced DNA damage induces FIR splicing [14]. The alternative splicing of *FIR* contributes to the transcriptional regulation of *c-myc*, which is critical for cell cycle control. Because Notch1 expression is pivotal for the pathogenesis of T-ALL, *TP53* or *c-myc* were knocked down using siRNA whereas BLM was treated as DNA damaging agent to examine the relationship among DNA damage, the alternative splicing of *FIR*, and cell cycle control. Knocking down both *TP53* and *c-myc* using siRNA significantly suppressed Notch1 expression without disturbing FIR expression (Figures 7A-C, arrows). TP53 expression was not affected significantly by the enforced expression by FIR//FIRΔexon2 using

Notch signaling pathway (Notch3, Hes1, Notch1, Dtx1, Ptcra: $p=1.35 \times 10^{-4}$) were more activated *in* $FIR^{+/-}TP53^{-/-}$ *(H635) than in* $FIR^{+/+}TP53^{-/-}$ *(N166) mouse.*

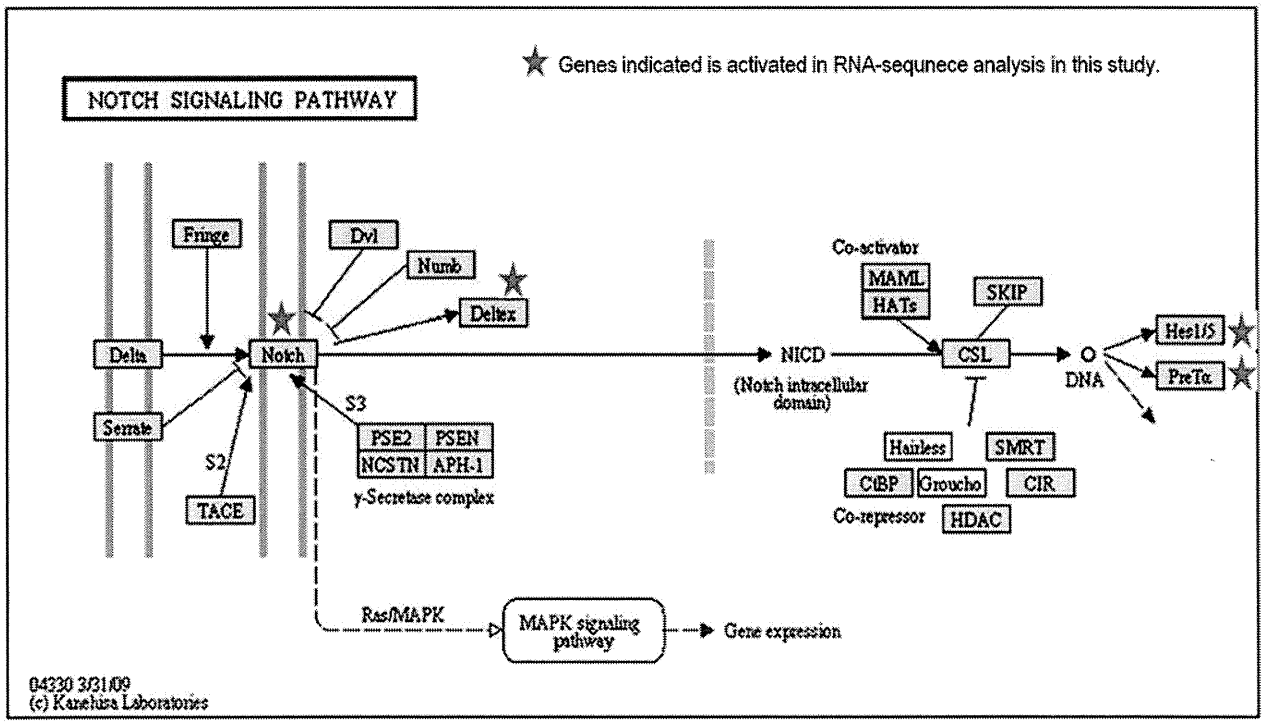

Figure 5: Signaling pathway activated in sorted thymic lymphoma cells in $FIR^{+/-}TP53^{-/-}$ mice. (A) KEGG pathway analysis showed that Notch Signaling pathway was more activated in $FIR^{+/-}TP53^{-/-}$ mice compared with $FIR^{+/-}TP53^{-/-}$ and $FIR^{+/+}TP53^{-/-}$ mice, with the *Notch3*, *Hes1*, *Notch1*, *Dtx1* and *Ptcra* genes upregulated ($P=1.4\times10^{-4}$). Other activated pathways were also shown in Figure S6.

an adenovirus vector (Figure 7D). DNA damage affects the alternative splicing of FIR, which contributes to the transcriptional activation of *c-myc* via a dominant negative effect on endogenous FIR [14]. Activated c-Myc accelerates the cell cycle by suppressing p27Kip1 expression, which leads to the accumulation of DNA damage [14, 15].These results suggest that disturbed *FIR* expression or the altered splicing of *FIR* may contribute to the pathogenesis of T-ALL via upregulating c-Myc-Notch1 axis independent on TP53 (Figure 7E). Therefore, *FIR* splicing is a novel mechanism that links DNA damage to *c-myc* regulation (Figure 7E).

DISCUSSION

The conditional $FIR^{+/-}$ mouse exhibited prominent

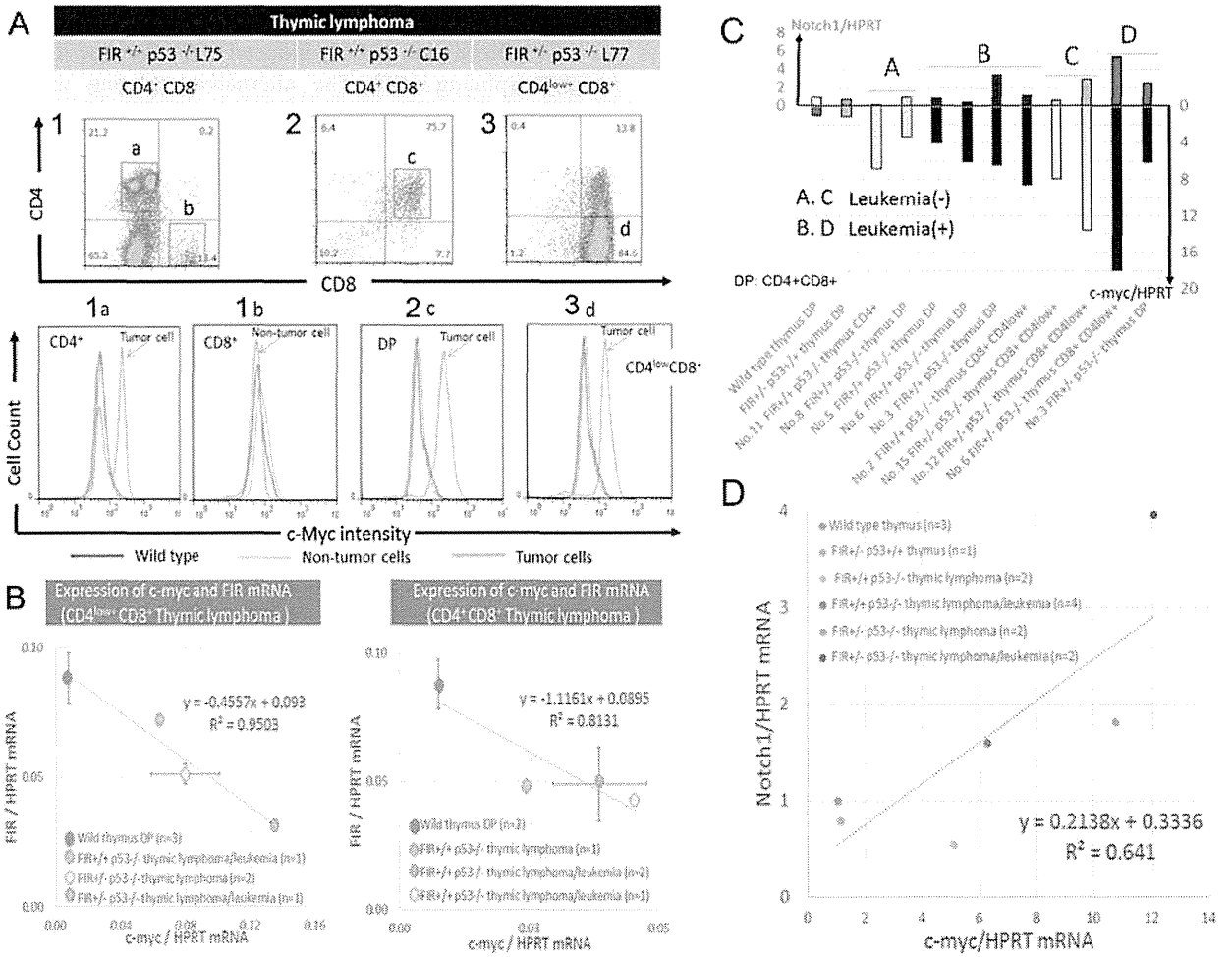

Figure 6: c-Myc protein is enhanced and showed inverse correlation with FIR in thymic lymphoma cells and promotes bone marrow invasion. (A) Flow cytometry of thymic lymphoma cells in $FIR^{+/+}P53^{-/-}$ or $FIR^{+/-}P53^{-/-}$ mice are indicated. $CD4^+$ cells of $FIR^{+/+}P53^{-/-}$ (upper column 1) has two populations indicated c-Myc-high (1a) and c-Myc–low intensity (1b). Notably, c-Myc-high (1a) population, presumably lymphoma cells, has c-Myc-low peak, indicating non-tumor cells cluster. $CD4^+CD8^+$ cells (2c) also indicated c-Myc-high intensity population. $CD4^{low+}CD8^+$ (3d) showed c-Myc-high intensity population indicated by FACS (bottom). Red line: Thymus cells of wild type $FIR^{+/+}P53^{+/+}$ mouse. Thin blue line: non-tumor cells of $FIR^{+/+}P53^{-/-}$ or $FIR^{+/-}P53^{-/-}$ mice. Orange line: Tumor cells of $FIR^{+/+}P53^{-/-}$ or $FIR^{+/-}P53^{-/-}$ mice. (B) Inverse correlation with significance between *c-myc* and FIR mRNA expression in $CD4^{low+}CD8^+$ or $CD4^+CD8^+$thymus lymphocytes obtained from $FIR^{+/+}P53^{-/-}$ or $FIR^{+/-}P53^{-/-}$ mice. Relative *c-myc* (or FIR)/HPRT mRNA expression of $CD4^{low+}CD8^+$ thymic lymphoma/leukemia cells of $FIR^{+/+}p53^{-/-}$ (light green) was 8.6 (0.81), thymic lymphoma cells of $FIR^{+/-}p53^{-/-}$ (yellow) was 10.7 (0.58) and thymic lymphoma/leukemia cells of $FIR^{-/-}p53^{-/-}$ (blue) was 18.0 (0.37) times as compare to thymic cells of wild mouse (dark orange), respectively (right). The relationship between *c-myc*/HPRT mRNA (x-axis) and FIR/HPRT mRNA (y-axis) was y=-0.4557x+0.093 (R^2=0.9503). Relative *c-myc* (or FIR)/HPRT mRNA expression of $CD4^+CD8^+$ thymic lymphoma cells of $FIR^{+/+}p53^{-/-}$ (light green) was 3.3 (0.56), thymic lymphoma/leukemia cells of $FIR^{+/-}p53^{-/-}$ (yellow) was 6.1 (0.48), and thymic lymphoma/leukemia cells of $FIR^{-/-}p53^{-/-}$ (blue) was 5.2 (0.56) times as compare to thymic cells of wild mouse (dark orange), respectively. The relationship between *c-myc*/HPRT mRNA (x-axis) and FIR/HPRT mRNA (y-axis) was y=-1.1161x+0.086 (R^2=0.8131). (C) (D) c-myc mRNA and Notch1 mRNA expression was positively correlated each other in sorted thymic lymphoma cells extracted from mice of different genetic backgrounds.

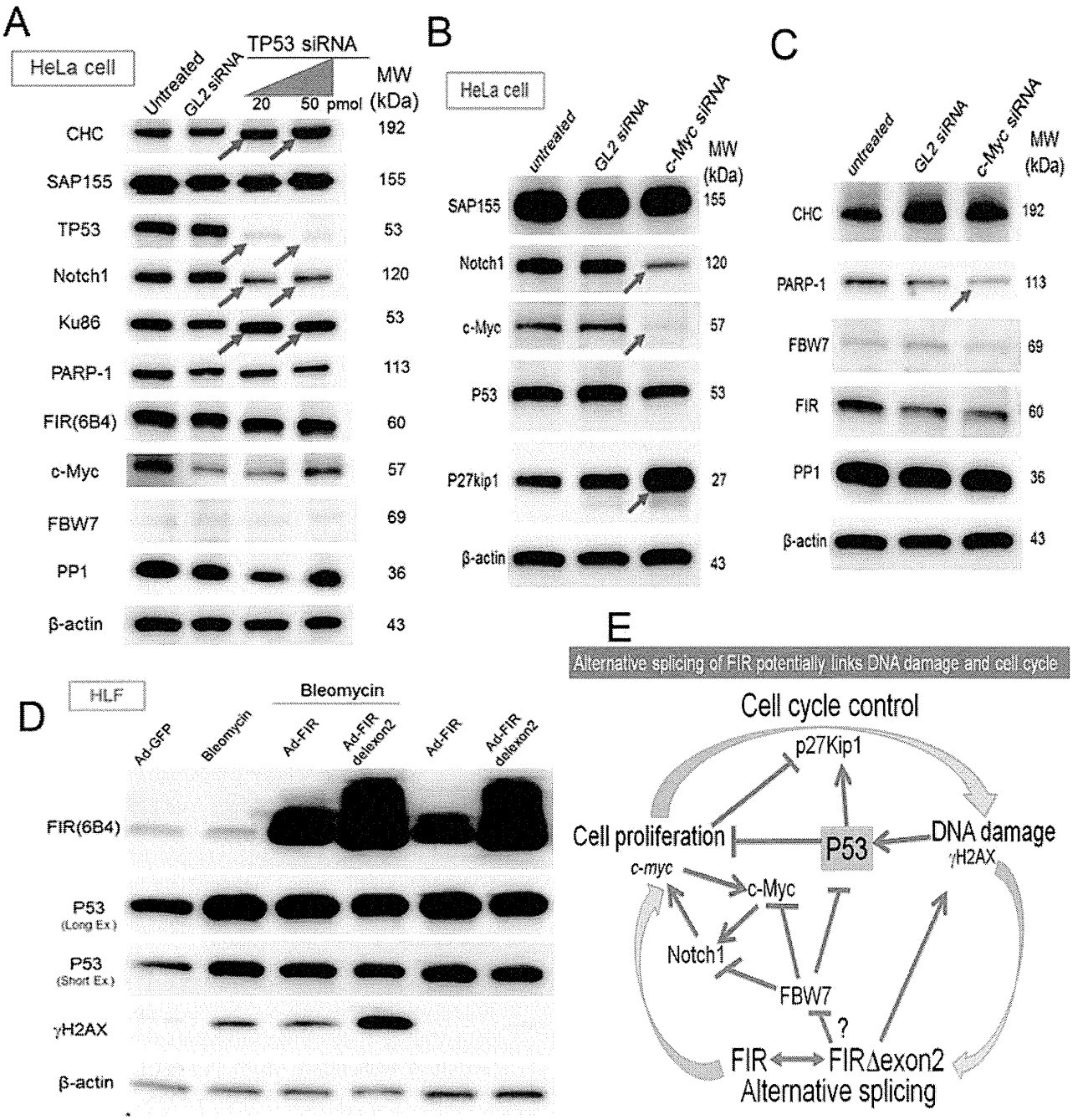

Figure7: Alternative splicing of FIR connects DNA damage response, *c-myc* activation and cell cycle control. (A) 20 and 50pmol of TP53 siRNA were transfected into HeLa cells. GL2 siRNA was transfected as the negative control. After 72h of incubation, whole-cell extracts were analyzed by western blotting for relevant protein expressions. (B, C) 20pmol c-Myc siRNA was transfected into HeLa cells. GL2 siRNA is for negative control. After 48h of incubation, whole-cell extracts were analyzed by western blotting for relevant protein expressions. (D) 3.76×10^8 VP/ml (10 MOI) of Ad-FIR or Ad-FIRΔexon2 adenovirus vectors and DNA damaging agent bleomycin (30 μg/ml) were either co-treated or single treated into HLF cell. 3.76×10^8 VP/ml (10 MOI) of GFP adenovirus (Ad-GFP) was treated as negative control. After 48h of incubation, whole-cell extracts were analyzed by western blotting. Severity of the DNA damage caused by bleomycin treatment is indicated by γH2AX expression. (E) Schematic view of haploinsufficiency, as a dominant negative-alternative splicing model of FIR in T-ALL pathogenesis. DNA damage affects alternative splicing of FIR that contributes to *c-myc* transcriptional activations. Activated c-Myc accelerates cell cycle by suppressing P27Kip1 and in turn accumulates DNA damage. The altered expression of FIRΔexon2 increased Notch1 at least partially by activating c-Myc via a TP53-independent pathway.

c-myc upregulation, particularly in the PB among other organs but without a significant pathogenic phenotype (Figure 1). The increased mRNA expression of *FIR/FIRΔexon2* was detected in human leukemia cell lines and clinical samples (Figure 1E–G). *FIR*$^{-/-}$ was embryonic lethal in mice before E9.5 (Table 1). *FIR*$^{+/-}$*TP53*$^{-/-}$ mice developed T-ALL (Figure 2) and exhibited an increased incidence of organ or bone marrow invasion (Figure 3). The bodyweight of *FIR*$^{+/-}$*TP53*$^{-/-}$ mice was less than that of *FIR*$^{+/+}$*TP53*$^{-/-}$ mice, and overall survival was reduced in *FIR*$^{+/-}$*TP53*$^{-/-}$ compared with that in *FIR*$^{+/+}$*TP53*$^{-/-}$ mice, presumably due to the rapid progression of T-ALL (Figure 4). The Notch signaling pathway was more activated in sorted CD4^{+}CD8^{+} thymic lymphoma cells isolated from *FIR*$^{+/-}$*TP53*$^{-/-}$ (H635) compared with those from *FIR*$^{+/+}$*TP53*$^{-/-}$ (N166) *mice,* as revealed by RNA-sequencing analysis (Figure 5*)*. Quantitative RT-PCR confirmed that *c-myc* mRNA expression was negatively correlated with *FIR* mRNA expression but positively correlated with *Notch1* mRNA in sorted T-ALL/thymic lymphoma cells (Figure 6). Furthermore, knocking down *TP53* or *c-myc* using siRNA suppressed Notch1 expression; however, TP53 expression was not affected significantly by the enforced expression of FIR/FIRΔexon2 using an adenovirus vector (Figures 7A–D). Thus, alternative splicing of FIR expression increased Notch1 through c-Myc upregulation independent on TP53-pathway (Figure 7E).

DNA damage affects alternative splicing by modulating the elongation activity and/or the phosphorylation status of RNA polymerase II [15,31]. In addition, BLM-induced DNA damage alters FIR splicing, which contributes to the transcriptional upregulation of *c-myc* via dominant negative effect on endogenous FIR [12, 13]. c-Myc accelerates the cell cycle by suppressing p27Kip1 expression, eventually leading to the accumulation of DNA damage. Therefore, FIR splicing is a novel mechanism that connects DNA damage to the regulation of *c-myc*. The sustained c-Myc and Notch1 protein expression level also needs to be regulated by their stability and degradation process. So, how does *FIR* splicing contribute to these processes that are pivotal for T-ALL pathogenesis? One possibility is that *FIR/FIRΔexon2* interferes with FBW7 (F-box WD repeat-containing protein 7). FBW7 is a polyubiquitin ligase that acts on Cdc4 phospho-degron (CPD) consensus sequence (--TP--S/E--)-containing proteins, including c-Myc and Notch1 [32-36]. Therefore, leukemic cells from FBW7-deficient mice exhibited the marked accumulation of Notch-1 and c-Myc proteins, which led to the development of T-ALL [25]. The WD-like motifs (W425 and D399) in the CPD-binding propeller pocket of FBW7 are positioned close to each other in the 3D structure after protein folding, and they potentially interact with FIR-UHM (LNGRWFAGRKVVA) (unpublished data). Purified FIRΔexon2 exhibited a higher binding affinity for Skp1-FWB7 than did FIR in a HiTrap Ni affinity column [37], suggesting that FIRΔexon2 may interact with FBW7 (data not shown). Therefore, FIRΔexon2 may sustain c-Myc protein levels post-transcriptionally by inhibiting the FBW7-mediated pathway. This situation is further complicated because the dimerization site of FIR (PUF60), the RRM2 domain, is not affected by the splicing of exon 2 or 5 in terms of FBP/FIR/FIRΔexon2/PUF60/SAP155 interaction [38, 39]. The difference of the FBP/FIR/FIRΔexon2/PUF60/SAP155 interaction or regulation among organs also needs to be revealed in carcinogenesis in further study.

The KRAS G12D and Notch1 mutations contribute cooperatively to the leukemogenic transformation of normal T-cells in mouse models [40]. Notch1 mutations, which activate *c-myc* transcription, were identified in > 50% of T-ALL cases [41-43], suggesting that upregulation of Notch1 or c-Myc phosphorylation occurred via the EGFR/KRAS/MEK/ERK pathway [37]. How does the splicing of FIR affect Notch1 or c-Myc phosphorylation? Phosphorylated-ERK (p-ERK) is a substrate of protein phosphatase 1 (PP1). Both Ad-FIR and Ad-FIRΔexon2 activated p-ERK but did not affect PP1 in Jurkat and HeLa cells (data not shown). Ad-FIRΔexon2, but not Ad-FIR, elevated pSer62-c-Myc expression much more than expected by *c-myc* mRNA level in HeLa cells [16]. Therefore, FIRΔexon2 sustains c-Myc activation via both transcriptional and post-transcriptional mechanisms. Notably, FLAG-tagged FIR or FIRΔexon2 were co-immunoprecipitated with TOPOII-alpha, SAP155, TRRAP, and filamine-A in pull-down assays [14, 18, 19]; these proteins contain the GKKRVRWADLE sequence, which is specific for interactions with PP1 [44]. Because PP1 inhibits the RAS/BRAF/MEK/ERK pathway [45] and also regulates c-Myc phosphorylation at Ser-62 (pSer62-c-Myc) [46], FIRΔexon2 may interfere with the function of PP1. However, further studies are required to reveal the detailed mechanism behind this potential effect.

Finally, five individuals had *de novo* interstitial 8q24.3 (chr8: 144,868,670–144,933,911; USCS Genome Browser hg19, http://genome.ucsc.edu.) deletions ranging from 65 kb to 1 Mb on the chromosome that encodes *Scrib* [scribbled homologue (MIM 607733)], *FIR* (PUF60), and *NRBP2* (nuclear receptor binding protein 2) [29]. Patients with 8q24.3 deletions showed clinical phenotypes associated with coloboma, congenital heart defects, limb abnormalities, psychomotor retardation, and convulsions; however, no hematologic malignancies or lymphoma have been described [30]. Detecting FIR/FIRΔexon2 for diagnosis, or the use of specific antibodies against FIRΔexon2 or chemicals that inhibit the FIR/FIRΔexon2/SAP155 interaction may have clinical applications in T-ALL.

Together, these data suggest that the alternative splicing of FIR may link DNA damage to *c-myc* regulation. Haploinsufficiency of the *c-myc* transcriptional

repressor *FIR* and the *FIR*$^{+/-}$*TP53*$^{-/-}$ genotype in mice potently promoted the progression of T-ALL/lymphoma, at least in part by activating the Notch signaling pathway with *c-myc*/c-Myc upergulation. The alternative splicing of *FIR* contributes to not only colorectal carcinogenesis but also leukemogenesis.

MATERIALS AND METHODS

Human leukemia samples

Human leukemia, control or adult healthy volunteer samples were obtained from Chiba University Hospital (adult patients) with written informed consent (Table S1).

Generation of animals and ethical approval

C57BL/6NCrSlc mice were obtained from Japan SLC. Mice were bred and maintained in the animal research facility of the Graduate School of Medicine, Chiba University (Chiba, Japan) in accordance with institutional guidelines. This study was approved by the institutional review committees of Chiba University. All experiments using mice received approval from the Chiba University Administrative Panel for Animal Care. Littermates were used as controls in all experiments.

Constructing the *FIR*-targeting vector

Construct of FIR targeting vector was indicated (Figures 1 and S1).

Homologous recombination of the *FIR*-targeting vector in ES cells

First, FIR targeting vector was injected by electroporation for homologous recombination ES cells into (C57BL/6) to prepare genetically modified ES cells (C57BL/6). 23 (clone nos. 26, 29, 31, 45, 84, 105, 112, 114, 117, 125, 145, 146, 172, 176, 178, 179, 185, 188, 191, 238, 244, 245, and 265) of 279 clones were identified in which the FIR-targeting vector had integrated in the chromosomes of ES cells using PCR (Figure S5A). The LoxP site of the integrated FIR-targeting vector was confirmed using PCR with suitable primers (Figure S5B). The integration of the FIR-targeted allele into the genome was confirmed using Southern blotting with 5′ and 3′ probes (Figure S5C). The FIR genomic sequence located between the loxP sites was excised using Cre-recombinase (Figure S5D). After verifying that the ES cells had integrated the FIR-targeting allele successfully using PCR and Southern blotting, the ES cells were microinjected into blastocysts from BALB/c mice. The resulting blastocysts were inoculated into the uterus of ICR mice (Table S2). Male FIR$^{fl/+}$ chimeric mice (chimera mouse) were cross-fertilized with C57BL/6 female mice to obtain F1 FIR heterozygous mice.

Generating inducible FIR heterozygous knockout mice, *FIR*$^{+/-}$

ES cells were purchased from DS Pharma Biomedical Co., Ltd. (Osaka, Japan). The FIR-targeting vector was prepared from Bac clone using PCR, and the FIR heterozygous knockout mice were prepared using the Cre-loxP system in C57BL6 mice [47] (Unitech Co., Ltd, Chiba, Japan) (Figure S1B). The primers and probes used to prepare FIR heterozygous knockout mice are shown in Figure 1A and Table S2. To assess the function of FIR in hematopoiesis, *FIR* was deleted conditionally by crossing *FIR*$^{fl/+}$ mice with *CAG-Cre* transgenic mice, which express *Cre* ubiquitously (*FIR*$^{+/-}$) (Figure S3). The efficient deletion of *FIR* in fetal cells from *FIR*$^{+/-}$ mice was confirmed using genomic PCR (Figure 1, primers loxP_F1, forward; and loxP_R2; reverse; Figure S6). The number of chimeric mice, born from clone number 26, 105 and 145 were indicated (Table S2). Genetically modified ES cells (C57BL/6) were microinjected into the blastocysts of BALB/c mice. Among the 23 positive clones that contained the FIR-targeting vector, clones 26, 105, and 145 (Figure S6C) were microinjected into the blastocyst cavity of BALB/c mice and were then transplanted into the uterus of pseudo-pregnant ICR mice. Seven chimeric mice were obtained successfully (Figure S6A and Table S2). Cross-fertilization was performed between male FIR$^{fl/+}$ (C57BL/6) and female C57BL/6 mouse to obtain the sperm carrying the FIR$^{fl/+}$ genome (Figure S6B). Finally, FIR$^{fl/+}$ mice were cross-fertilized with CAG-Cre transgenic mice to obtain FIR$^{fl/+}$/Cre(+), which were conditionally inducible FIR heterozygous knockout (*FIR*$^{+/-}$) mice (Figure S6C). FIR heterozygous knockout mice were confirmed using the Cre-LoxP system (Figure S6D).

Southern blotting of genomic DNA

Three probes were prepared and used for Southern blotting. The 5′-probe (new probe) was located upstream of the short arm in the neomycin gene, and the 3′-probe was located downstream of the long arm (Figure S1). The primers and qRT-PCR conditions used for Southern blotting are shown in Table S5A.